
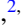


Complex networks of interacting stochastic tipping elements: Cooperativity of phase separation in the large-system limit

Jan Kohler,^{1,2} Nico Wunderling ^{2,3,4,*} Jonathan F. Donges ^{2,5} and Jürgen Vollmer^{1,†}

¹*Institute for Theoretical Physics, University of Leipzig, 04103 Leipzig, Germany, EU*

²*Earth System Analysis, Potsdam-Institute for Climate Impact Research, Member of the Leibniz Association, 14473 Potsdam, Germany, EU*

³*Institute of Physics and Astronomy, University of Potsdam, 14476 Potsdam, Germany, EU*

⁴*Department of Physics, Humboldt University of Berlin, 12489 Berlin, Germany, EU*

⁵*Stockholm Resilience Centre, Stockholm University, 10691 Stockholm, Sweden, EU*



(Received 13 April 2021; accepted 26 August 2021; published 1 October 2021)

Tipping elements in the Earth system have received increased scientific attention over recent years due to their nonlinear behavior and the risks of abrupt state changes. While being stable over a large range of parameters, a tipping element undergoes a drastic shift in its state upon an additional small parameter change when close to its tipping point. Recently, the focus of research broadened towards emergent behavior in networks of tipping elements, like global tipping cascades triggered by local perturbations. Here, we analyze the response to the perturbation of a single node in a system that initially resides in an unstable equilibrium. The evolution is described in terms of coupled nonlinear equations for the cumulants of the distribution of the elements. We show that drift terms acting on individual elements and offsets in the coupling strength are subdominant in the limit of large networks, and we derive an analytical prediction for the evolution of the expectation (i.e., the first cumulant). It behaves like a single aggregated tipping element characterized by a dimensionless parameter that accounts for the network size, its overall connectivity, and the average coupling strength. The resulting predictions are in excellent agreement with numerical data for Erdős-Rényi, Barabási-Albert, and Watts-Strogatz networks of different size and with different coupling parameters.

DOI: [10.1103/PhysRevE.104.044301](https://doi.org/10.1103/PhysRevE.104.044301)

I. INTRODUCTION

Hysteresis is a hallmark of first-order phase transitions. For thermodynamic systems it leads to supercooling and superheating with subsequent explosive phase changes [1,2]. These rapid changes are well-understood for common thermodynamic phase transitions (see, e.g., [3–5]). However, they still pose challenges for systems with nonstandard interaction rules, like the Achlioptas Process [6–10], or nonstandard interaction topologies like processes on networks, where hysteresis can lead to cascading failure [11–14]. Hysteresis and explosive transitions between (meta)stable states are also commonly observed in other systems. In ecological and climate systems [15], and in finance, economics, and politics [16], they are commonly denoted as tipping processes. Further applications are discussed in the recent reviews [12,17].

The present study is inspired by current models of climate change that are formulated in terms of networks of interacting tipping elements [18–25]. The interactions provide long-lived metastable states and rapid cooperative transitions between the states. Often such a stabilization and cooperation in a tipping event is caused by positive feedback effects, i.e., coupling or interactions that tend to align individual elements.

For ferromagnetic systems the interaction tends to align individual spins with the molecular field. An example in the Earth system is the surface albedo of sea ice [26,27]. A decrease in the ice-covered surface area due to an increase in global mean temperature decreases the surface albedo. This, in turn, increases the temperature and causes higher rates of melting [28,29]. The interaction between the elements leads to *cascading* behavior when the abrupt state shift of an element causes the tipping of another [30]. The resulting rapid nonlinear changes of the climate were predicted almost 40 years ago [31]. Early on they were investigated regarding a snowball-Earth/warm-Earth-state transition [32–35], and more recently a transition towards a potential *hothouse* state [15,23].

The present paper adds to the ongoing research on the dynamic behavior of coupled tipping elements by identifying universal behavior in the tipping of large-scale systems. Tipping in a network comprising a large number of tipping elements will be characterized by the first two cumulants (expectation and variance) of the distribution of tipping elements. In large networks, the expectation behaves like a single aggregated tipping element. Moreover, the variance remains small, and for small noise it rapidly decays except for an initial transient growth early on. Hence, we adopted the expectation as an order parameter of the transition, and we will show that the tipping dynamics depends only on two dimensionless control parameters. These parameters take an analogous rise to the temperature and the external field in the thermodynamic treatment of magnetic phase transitions [36].

* Author to whom all correspondence should be addressed: wunderling@pik-potsdam.de

† juergen.vollmer@uni-leipzig.de

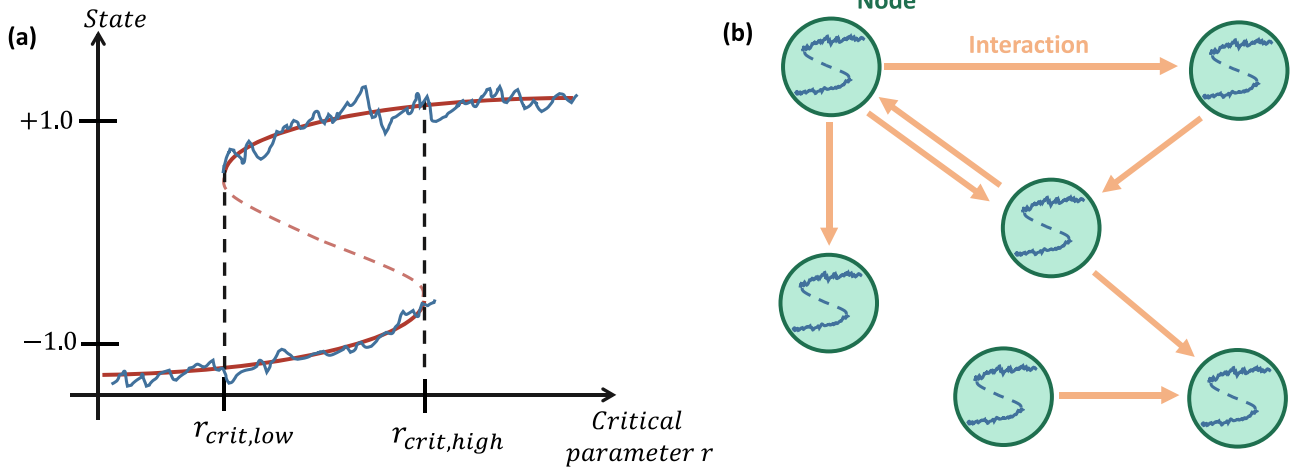


FIG. 1. Dynamics of the nodes in a network of tipping elements. (a) Bifurcation diagram of Eq. (1) where solid and dashed red lines show the positions of the stable and unstable steady states, respectively. In the range between $r_{\text{crit,low}}$ and $r_{\text{crit,high}}$ there are two stable states and one unstable state. At the borders of the interval, a stable state merges with the unstable state, and they disappear in a saddle-node bifurcation, and systems at that position will decay to the remaining stable state. The trembling blue line illustrates the stochastic fluctuations around the stable state that we are using here; see Eq. (2a). (b) Nodes in an exemplary network of interacting tipping elements [see Eq. (2a)], where each node is of the form shown in panel (a).

The paper is organized as follows. In Sec. II we introduce the system of nonlinear differential equations that are analyzed in the present study, and we describe how they are coupled in network structures. Moreover, we also describe how the systems are simulated. In Sec. III we present our main results. First, the cumulants of the distribution of states of a network of unbiased tipping elements are defined, and their time evolution is derived (Sec. III A). Then, we introduce rescaled coordinates that allow us to discuss universal aspects of the late-time dynamics (Sec. III B). In Sec. IV the dynamics of the expectation is worked out and compared to numerical data. Section V addresses the impact of additional forcing terms (bias) and offsets in the coupling coefficients. In Sec. VI, we discuss the main findings of our work, its relations to other work, and we suggest follow-up work. Section VII concludes the paper with an exposition of our most important findings.

II. THEORY AND METHODS

The present study addresses the collective response of N tipping elements that are coupled linearly through network links distributed according to paradigmatic network types (Erdős-Rényi, Barabási-Albert, and Watts-Strogatz). The tipping elements are described by a system of differential equations adapted from Refs. [24,25] using the software package PYCASCADES [37]. A Gaussian white noise is applied to the tipping elements to model stochastic fluctuations.

A. Equations of motion

Many natural systems show tipping paired with hysteresis-like behavior [16]. The behavior of such a tipping element is commonly modeled by cubic differential equations [24,25,38] with normal form [39],

$$\frac{dx}{dt} = -x^3 + x + r, \quad (1)$$

where r is the bifurcation parameter. The system is in a bistable state when its right-hand side has three roots, i.e., for $r \in (r_{\text{crit,low}}, r_{\text{crit,high}}) = (-\sqrt{4/27}, \sqrt{4/27})$. At $r_{\text{crit,low}}$ and $r_{\text{crit,high}}$ two of the roots disappear in a saddle-node bifurcation. The bifurcation diagram of a single node including noise is shown in Fig. 1(a).

Commonly, tipping elements are not isolated. For instance, Krönke *et al.* [25] suggested to study the dynamics of N coupled tipping elements $k \in \{1, \dots, N\}$ that are linearly coupled to other nodes $l \neq k$ [see Fig. 1(b)],

$$\frac{dx_k}{dt} = -x_k^3 + x_k + \sum_l' d_{kl}x_l + \xi \frac{dW_k}{dt}. \quad (2a)$$

The prime at the sum indicates that l takes values in $l \in \{1, \dots, N\} \setminus \{k\}$. On average, a node k is coupled to pN other elements. W_k denotes a Wiener process and ξ is the strength of the noise.

Equation (2) describes homogeneous systems where all nodes follow the same dynamics and have the same critical parameter values for tipping. Such systems are discussed in Secs. III and IV. In Sec. V we expand that discussion to treat dynamics with additional drift terms, d_k , and offset terms, r_{kl} ,

$$\frac{dx_k}{dt} = -x_k^3 + x_k + d_k + \sum_l' d_{kl}(x_l - r_{kl}) + \xi \frac{dW_k}{dt}. \quad (2b)$$

B. Network topologies

There is ample room for different types of interaction networks when one only specifies that a node is connected to $p(N-1)$ other nodes on average. We will therefore consider three types of networks to explore the impact of the structure of the interaction network on the tipping dynamics:

ER: The connections form an Erdős-Rényi network [40] when they are assigned randomly with probability p . The

probability distribution to be connected to m nodes, i.e., the degree distribution, amounts to a binomial distribution.

BA: Barabási-Albert networks [41] are built by sequentially adding connections under the constraint of preferential attachment: elements with a higher number of connections have a larger chance to receive more links. This leads to scale-free networks where the degree distribution has a power-law tail that decays like m^{-3} .

WS: Watts-Strogatz [42] networks are built by arranging the elements as a one-dimensional ring, where each node is connected to its pN nearest neighbors. Subsequently, a fraction β of the links is reconnected at random to a new element. This generates networks with the small-world property.

C. Numerical methods

Tipping behavior in ER, BA, and WS networks has been analyzed previously by Krönke *et al.* [25]. Wunderling *et al.* [37] developed the PYTHON package PYCASCADES to create the directed network of coupled tipping elements with the PYTHON NETWORKX2.3 package [43] and analyze the dynamics of tipping cascades based on the package SDEINT [44] for the integration of stochastic differential equations. These programs are used here to generate the networks and integrate the stochastic differential equations (2a). If not stated otherwise, the system is integrated up to $t = 100$, using a step size of $\Delta t = 0.01$. The coupling strengths d_{kl} will be drawn from a uniform distribution with $0 < d_{kl} < 2d$.

In the simulation runs, the nodes are initially placed at $x = 0$, i.e., the unstable fixed point, and the cascade is started by setting v nodes to $x = 1$. Thus, we focus on the transient behavior of tipping.

At times, the noise turns the point $x = 0$ into a stable fixed point of the dynamics [45]. Then, we study cases in which the coupling of the system is strong enough such that all nodes follow the initial displacement of the displaced node.

III. MEAN-FIELD EVOLUTION

We characterize the state of the network of tipping elements by the expectation of the state x_k of the elements,

$$\bar{x} = \langle x_k \rangle = \frac{1}{N} \sum_{k=1}^N x_k, \tag{3a}$$

and by their variance,

$$\bar{v} = \langle (x_k - \bar{x})^2 \rangle = \langle y_k^2 \rangle, \tag{3b}$$

where $y_k = x_k - \bar{x}$ denotes the deviation of x_k from the expectation \bar{x} . In Sec. III A we derive the equations for the time evolution of x and v that derive from Eq. (2a). To this end, we adopt a closure where we suppress higher-order moments and correlations. Then we point out universal aspects of the time evolution towards the asymptotic steady state (Sec. III B).

A. Moment expansion

To evaluate the time evolution of the cumulants of the x_k distribution, we note that taking averages $\langle _ \rangle$ is a linear oper-

ation such that it commutes with taking the time derivative,

$$\begin{aligned} \dot{\bar{x}} &= \frac{d}{dt} \langle x_k \rangle = \langle \dot{x}_k \rangle, \\ \dot{\bar{v}} &= \frac{d}{dt} \langle y_k^2 \rangle = 2 \langle y_k \dot{x}_k \rangle. \end{aligned}$$

To evaluate the averages, we express Eq. (2a) as

$$\begin{aligned} \dot{x}_k &= -(\bar{x} + y_k)^3 + \bar{x} + y_k + \sum_l' d_{kl}(\bar{x} + y_l) + \xi \frac{dW_k}{dt} \\ &= \bar{x} \left(1 - \bar{x}^2 + \sum_l' d_{kl} \right) + y_k (1 - 3\bar{x}^2) - 3\bar{x} y_k^2 \\ &\quad - y_k^3 + \sum_l' d_{kl} y_l + \xi \frac{dW_k}{dt}. \end{aligned} \tag{4}$$

Taking the average of Eq. (4) and observing that $\langle y_k \rangle = 0$ provides

$$\begin{aligned} \dot{\bar{x}} &= \bar{x} \left(1 - \bar{x}^2 - 3\bar{v} + \left\langle \sum_l' d_{kl} \right\rangle \right) \\ &\quad - \langle y_k^3 \rangle + \left\langle \sum_l' d_{kl} y_l \right\rangle + \left\langle \xi \frac{dW_k}{dt} \right\rangle. \end{aligned} \tag{5}$$

The expressions in the second line of this equation account for the third cumulant of the distribution of the state variables x_k , a biased average of the deviations y_k from the average of the state variables, and the impact of noise on the dynamics, respectively. In the present study, we consider a closure of the dynamics where the third cumulant and the biased average will be suppressed. Moreover, we focus on the average behavior of an ensemble of systems, where we perform two averages at the same time: (i) we average over the coupling strength in the network realizations, and (ii) we average over the noise W_k . Hence, the noise term vanishes, and $\langle \sum_l' d_{kl} \rangle$ takes the value $p(N - 1)d$, since each node is connected to $p(N - 1)$ other nodes with an average coupling strength d . Potential subtleties involved in taking the different averages will be addressed in a forthcoming paper. Altogether, we thus find

$$\dot{\bar{x}} = \bar{x} (1 + p(N - 1)d - \bar{x}^2 - 3\bar{v}). \tag{6a}$$

The evolution of v is obtained by multiplying Eq. (4) by $2y_k$ and taking the average,

$$\begin{aligned} \dot{\bar{v}} &= 2 \langle y_k \dot{x}_k \rangle = 2\bar{v} (1 - 3\bar{x}^2) + \left\langle y_k \xi \frac{dW_k}{dt} \right\rangle \\ &\quad - 6\bar{x} \langle y_k^3 \rangle - 2 \langle y_k^4 \rangle + 2 \left\langle \sum_l' d_{kl} y_k y_l \right\rangle. \end{aligned}$$

The term involving noise vanishes on account of considering a small-noise limit of the dynamics. The terms in the second row of the equation are higher-order moments and correlations that are dropped due to the assumptions of our closure of the moment hierarchy. Hence, we obtain

$$\dot{\bar{v}} = 2\bar{v} (1 - 3\bar{x}^2). \tag{6b}$$

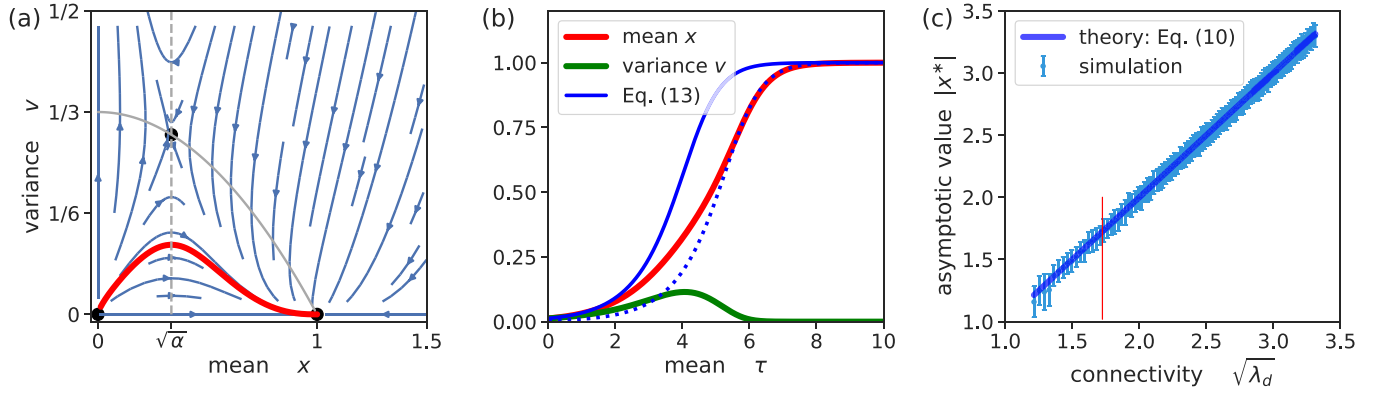


FIG. 2. Asymptotic values of the evolution. (a) Phase-space flow of the dynamical system, Eq. (9), for $\sqrt{\alpha} \simeq 1/3$. The analytical solutions of the nullclines are marked by gray lines, and fixed points are marked by black circles. The red line shows the numerical solution for $N = 80$ tipping elements that are connected by an ER network with $d = 0.1$ and $p = 0.25$. The numerical solutions for the blue vectors have been computed using the function `matplotlib.pyplot.streamplot` in PYTHON. The red and the green lines show the time evolution of the expectation and the variance of the numerical solution shown in panel (a). The thinner blue line shows the prediction, Eq. (13), for $x(0) = 1/N$ (for an explanation see Sec. IV B). The dotted line shows the same function shifted by $\Delta\tau = 1.24$. The shifted curve provides an excellent description of the late-time evolution of the expectation. (c) The data points show the asymptotic values x^* of numerical simulations of Eq. (2a) with $p = 0.25$ and couplings d_{kl} drawn from a uniform distribution $d_{kl} \in (0, 0.2)$. Error bars indicate the standard deviation derived from 50 realizations of the network configuration and the noise. The connectivity λ_d is varied by increasing N from 20 to 400 [cf. Eq. (7)]. The numerical values agree very well with the prediction Eq. (10) that is shown by a solid blue line. The parameter value of the trajectory shown in panels (a) and (b) is indicated by a vertical red line. For small networks, the system occasionally tips into the direction opposite to the perturbation. Hence, we plot the absolute value of x^* .

B. Asymptotics of the order parameter

The dynamics, Eq. (6), involves a single dimensionless parameter,

$$\lambda_d = 1 + p(N-1)d, \quad (7)$$

that depends on the average number of connections, $p(N-1)$, of a tipping element and on the average coupling strength, d . Hence, we denote it as *connectivity*.

Rescaled variables that are based on the connectivity will allow us to discuss the asymptotics of the order parameter in a more transparent form,

$$\begin{aligned} x(\tau) &= \bar{x}/\sqrt{\lambda_d}, \\ y(\tau) &= \bar{v}/\lambda_d, \\ \tau &= \lambda_d t. \end{aligned} \quad (8)$$

Denoting the derivatives of $x(\tau)$ and $y(\tau)$ with respect to τ as \dot{x} and \dot{y} provides

$$\dot{x} = \frac{dx}{d\tau} = x(1-x^2-3y), \quad (9a)$$

$$\dot{y} = \frac{dy}{d\tau} = 6y(\alpha-x^2), \quad (9b)$$

where $\alpha = (3\lambda_d)^{-1}$.

In Fig. 2(a) we show the phase-space flow of Eq. (9). The evolution has nullclines with $\dot{x} = 0$ at $x = 0$ and $y = (1-x^2)/2$ that are marked by solid gray lines. The nullclines with $\dot{y} = 0$ lie at $y = 0$ and $x = \sqrt{\alpha}$. They are marked by dashed lines. The three fixed points, $p_0 = (0, 0)$, $(\sqrt{\alpha}, (1-\alpha)/3)$, and $(1, 0)$, are located at the intersections of the $\dot{y} = 0$ and $\dot{x} = 0$ nullclines.

By inspection of the flow crossing the nullclines, one readily verifies that the fixed point p_i has i stable directions. For all

$\alpha > 0$, the trajectories approach a state with $x = \pm 1$ and vanishing variance. A representative sample trajectory is given by a solid red line in Fig. 2(a). Panel (b) shows the time evolution of $x(\tau)$ (red line) and $v(\tau)$ (green line) of this trajectory.

The approach towards the stable fixed point at $x = 1$ implies that

$$x^* = \lim_{\tau \rightarrow \infty} \bar{x} = \sqrt{\lambda_d} = \sqrt{1 + dp(N-1)}. \quad (10)$$

Fig. 2(c) shows that this dependence is indeed observed by our numerical data. Only for small connectivities, λ_d , do the data tend to lie closely below the prediction. We will come back to this point when we discuss Fig. 4.

IV. LATE-TIME EVOLUTION

The $\dot{x} = 0$ nullcline always takes the same form [solid gray line in Fig. 2(a)], while the $\dot{y} = 0$ nullcline is a vertical (dashed) line whose position, $x_c = \sqrt{\alpha} = (3\lambda_d)^{-1/2}$, depends on the system parameters. For trajectories that proceed to the left of x_c , the order parameter x remains small while v diverges. This behavior is unphysical and it lies outside of the scope of our model because our closure assumption can only be expected to work for small v . However, for large N the fixed point p_1 lies very close to $(0, 1/3)$, and we only consider initial conditions where $0 < v < x \ll 1$. For these initial conditions, one encounters trajectories as shown by a solid red line. Its x coordinates grows monotonically from 0 towards 1. Initially, the variance grows rapidly. Subsequently (after crossing the nullcline at $x = \sqrt{\alpha}$) it decays towards zero. For larger networks ($N \gg 1$) and for more strongly coupled networks (increasing pd) the crossover arises very close to zero ($\sqrt{\alpha} = [3(N-1)pd]^{-1/2} \ll 1$), and the maximum value of the variance decreases.

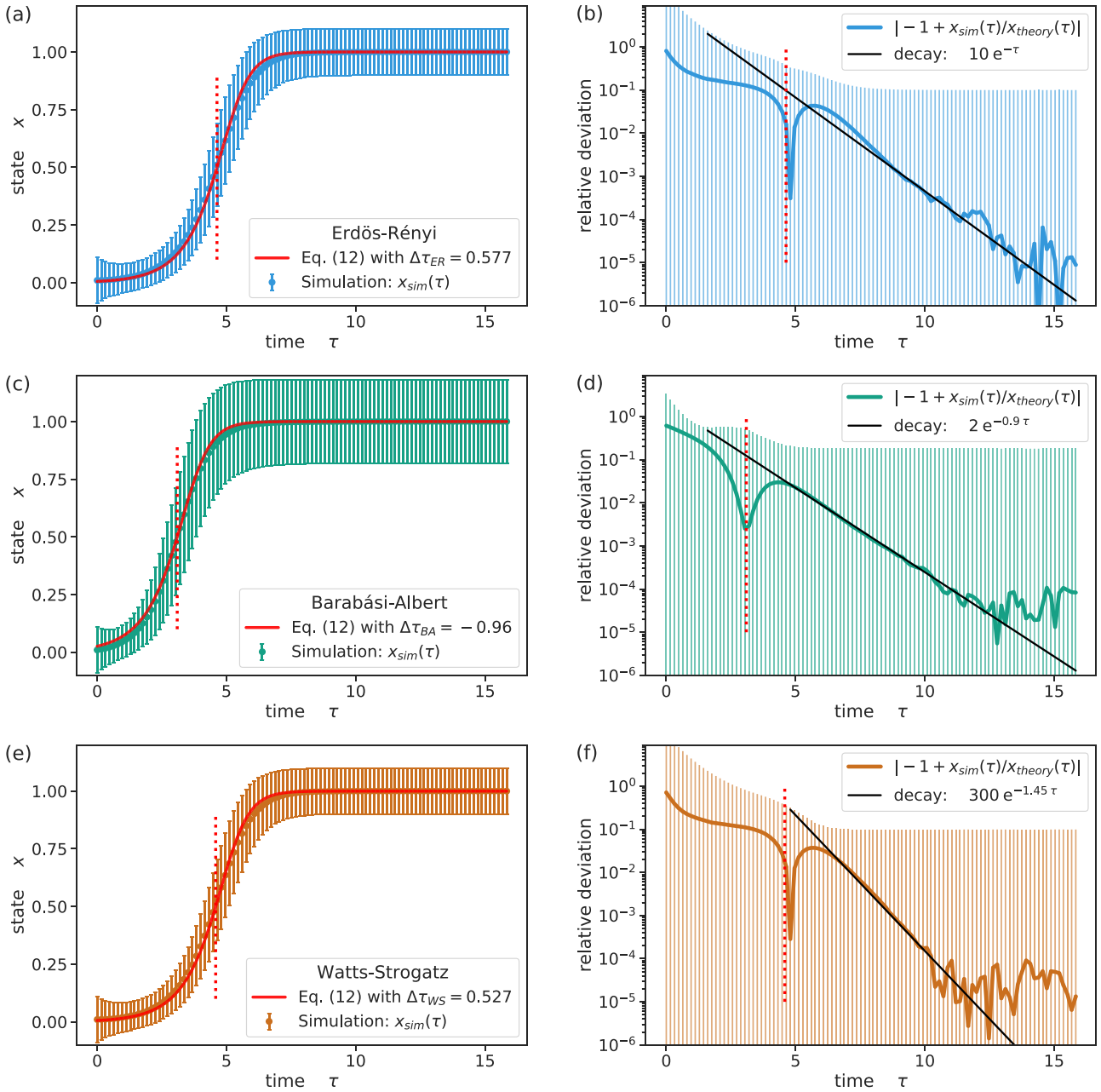


FIG. 3. Collective tipping behavior of different network types. The left and right panels show the evolution of the order parameter and relative deviation of numerical data from Eq. (2a) and the prediction from Eq. (13). The rows show data for (a,b) Erdős-Rényi, (c,d) Barabási-Albert, and (e,f) Watts-Strogatz networks with reconnection probability $\beta = 0.8$. The other parameters of the simulations are fixed to $N = 100$, $p = 0.1$, $d = 1.5$, and $\xi = 0.1$, such that $\lambda_d \simeq 16$. The data points and the error bars represent the expectation and the standard deviation over 50 realizations of the network and the noise, respectively. The prediction, Eq. (13), is indicated by a solid line in the left panels. It is shifted by $\Delta\tau$ to match the data at $x = 0.5$ (see the main text for details).

A. Approach to the stable fixed point

The approach towards p_2 is governed by the linearized Eq. (9) of the deviations $\epsilon = x - 1$ and v from the fixed point. We take into account that $\alpha \simeq 1/3$ for large connectivity, λ_d , and we find

$$\begin{pmatrix} \dot{\epsilon} \\ \dot{v} \end{pmatrix} \simeq \begin{pmatrix} -2 & -3 \\ 0 & -4 \end{pmatrix} \begin{pmatrix} \epsilon \\ v \end{pmatrix}. \quad (11)$$

The eigenvalue for the decay in v is therefore twice as large as the one in x , such that $v \sim (1 - x)^2$ close to the fixed point, in line with the flow lines of the phase-space plot shown in Fig. 2(a).

To discuss the evolution of x , we introduce the variable $w = x^2$ and observe that

$$\dot{w} = 2w(1 - w - 3v), \quad (12a)$$

$$\dot{v} = 2v(1 - 3w). \quad (12b)$$

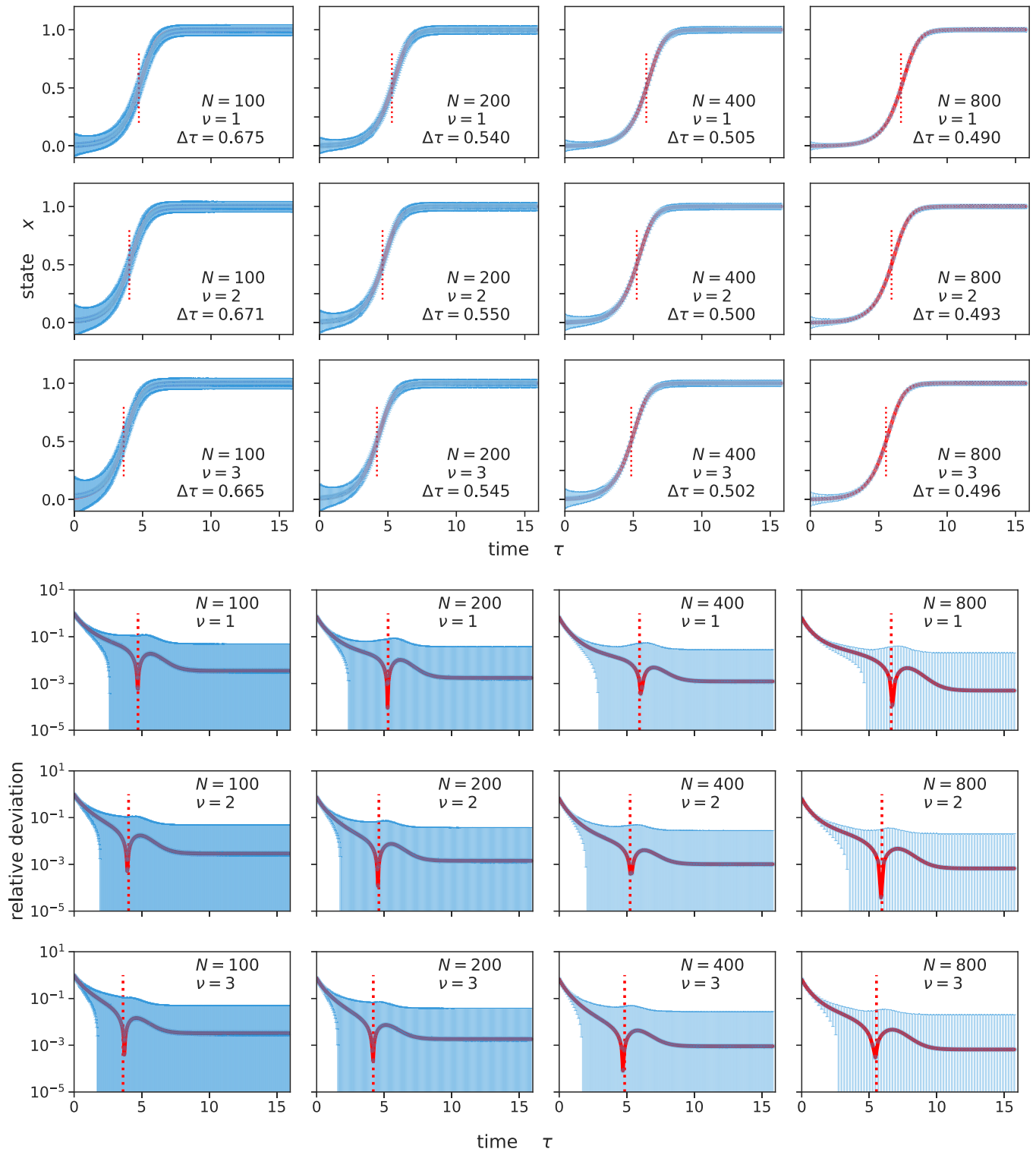


FIG. 4. Trajectories for different initial displacements $x(0) = \nu/N$. Calculations using Eq. (2a) have been conducted for ER networks with $d = 0.1$, $p = 0.25$, $\xi = 0.1$, $N \in \{100, 200, 300, 800\}$, and $\nu \in \{1, 2, 3\}$, with couplings d_{kl} drawn from a uniform distribution $d_{kl} \in (0, 0.2)$. This amounts to connectivities of $\lambda_d = 3.475, 5.975, 10.975$, and 20.975 , respectively. The data and their error bars in the upper panels represent the expectation and standard deviation of 100 simulations runs with independent realizations of the network and the noise. The corresponding lower panels show the relative deviation of the trajectory from the prediction Eq. (15) with $x_0 = \nu/N$ and a time shift $\Delta\tau$ provided in the respective legends.

The evolution of $w(\tau)$ for identically vanishing variance, $v \equiv 0$, is readily obtained by variable separation and partial fraction decomposition,

$$2\tau = \int_{w(0)}^{w(\tau)} \frac{dw}{w(1-w)} = \int_{w(0)}^{w(\tau)} dw \left[\frac{1}{w} + \frac{1}{1-w} \right] \\ = \ln \left[\frac{w(\tau)}{w(0)} \frac{1-w(0)}{1-w(\tau)} \right],$$

such that

$$x(\tau) = \sqrt{w(\tau)} = \left[1 + \frac{1-x^2(0)}{x^2(0)} e^{-2\tau} \right]^{-1/2}. \quad (13)$$

For late times, $\tau \gg 1$, we hence obtain the expected exponential decay

$$1-x(\tau) \simeq \frac{1-x^2(0)}{2x^2(0)} e^{-2\tau} \quad \text{for } \tau \gg 1. \quad (14)$$

To discuss the impact of finite values of v , we look for the solutions of Eq. (12) for $w = 1 - \varepsilon$, where

$$\dot{\varepsilon} = -2\varepsilon(1-\varepsilon) - 6v(1-\varepsilon), \\ \dot{v} = -4v\left(1 + \frac{3}{2}\varepsilon\right).$$

We approximate the equation for $\dot{\varepsilon}$ by inserting $v = c\varepsilon^2$ [cf. the discussion of the relation of v and ε below Eq. (11)], and we consider terms only until order ε^3 and $v\varepsilon$. As a consequence,

$$(1+3c)\dot{\varepsilon} = -2(1+3c)\varepsilon(1-(1+3c)\varepsilon)$$

such that $\varepsilon(\tau) = 1-x(\tau)$ remains unchanged up to multiplication by the factor $1+3c$. However, in view of Eq. (14), such a factor can be accounted for by a shift, $\Delta\tau$, of time, yielding the following prediction for the time evolution of the order parameter:

$$x_{\text{theory}}(\tau) \simeq \left[1 + \frac{1-x^2(0)}{x^2(0)} e^{-2(\tau-\Delta\tau)} \right]^{-1/2}. \quad (15)$$

This expression has a single free parameter $\Delta\tau$ that amounts to a time delay to reach the half-time $\tau_{1/2}$, where $x_{\text{theory}}(\tau_{1/2}) = 1/2$,

$$\tau_{1/2} = \Delta\tau - \frac{1}{2} \ln \frac{3x^2(0)}{1-x^2(0)}. \quad (16)$$

B. Numerical test of Eq. (15)

The left columns of Fig. 3 show the evolution of the order parameter for ER, BA, and WS networks. As an initial condition we consider a system where one node, say ℓ , is displaced to a value $x_\ell = \sqrt{\lambda_d}$, and all other nodes, $m \neq \ell$, start at $x_m = 0$. This amounts to initial conditions with

$$x(0) = \frac{\langle x_k \rangle_{\tau=0}}{\sqrt{\lambda_d}} = \frac{1}{\sqrt{\lambda_d}} \frac{1}{N} \sum_{k=1}^N x_k(0) \\ = \frac{0 \times (N-1) + 1 \times \sqrt{\lambda_d}}{N \sqrt{\lambda_d}} = \frac{1}{N}.$$

For each type of network, we perform 50 runs with different realizations of the networks and noise. The expectation of the

order parameter, x_{sim} , for the resulting evolution is given by a circle, and the error bars mark the standard deviation over the simulation runs.

The theoretical prediction, x_{theory} , is provided by a solid line. The time offsets are determined such that the numerical data and theoretical prediction match for $x = 1/2$. In a logarithmic plot of the relative deviation $(x_{\text{sim}}/x_{\text{theory}})/x_{\text{theory}}$ [Figs. 3(b), 3(d) and 3(f)] this results in a singularity at time $\tau_{1/2}$ that is marked by vertical dotted lines. The lines align with the singularity for

$$\Delta\tau_{\text{ER}} = 0.577, \\ \Delta\tau_{\text{BA}} = -0.96, \\ \Delta\tau_{\text{WS}} = 0.527. \quad (17)$$

ER and WS networks have very similar time offsets of about $\Delta\tau \simeq 0.5$. In contrast, BA networks decay significantly faster. The negative value of $\Delta\tau_{\text{BA}}$ implies that these networks decay even faster than predicted by the $v = 0$ result, Eq. (13). Follow-up work will have to clarify if and how this intriguing finding is related to the existence of hubs in BA networks, nodes with a degree greatly exceeding the average.

In addition to the position of $\tau_{1/2}$, Figs. 3(b), 3(d) and 3(f) demonstrate that the prediction, Eq. (15), provides an excellent description of the data for times beyond $\tau_{1/2}$. The time offset $\Delta\tau$ is the only fitting parameter in this description.

C. Influence of initial displacement

In the previous sections, one node has been perturbed by a fixed value initially. To discuss the effect of larger initial perturbations, we explore now systems where initially ν nodes are tipped to the asymptotic equilibrium value $x^* = \sqrt{\lambda_d}$. Consequently,

$$x(0) = \frac{\langle x_k \rangle_{t=0}}{\sqrt{\lambda_d}} = \frac{1}{\sqrt{\lambda_d}} \frac{1}{N} \sum_{k=1}^N x_k(0) \\ = \frac{0 \times (N-\nu) + \nu \times \sqrt{\lambda_d}}{N \sqrt{\lambda_d}} = \frac{\nu}{N}. \quad (18)$$

According to Eq. (15), this change in $x(0)$ will be the only change in x_{theory} . This prediction is scrutinized in Fig. 4 where we show data for ER networks with 100, 200, 400, and 800 nodes, where we excited initially $\nu = 1, 2, \text{ or } 3$ nodes:

(i) For a given value of N the time offsets for different ν are indeed constant to within our numerical accuracy. Moreover, the positions of the dotted lines clearly show the decrease of $\tau_{1/2}$ that is predicted by Eq. (16).

(ii) For increasing N the time offset decreases. This is in line with the expectation that the variance reaches smaller values for increasing λ_d such that the dynamics more closely follows the $v = 0$ dynamics.

(iii) The relative deviation does not decay to zero. Indeed, at second glance one recognizes that the data in Fig. 3 also tend to saturate at a 10^{-5} level. Hence, the data do not quite saturate at $\sqrt{\lambda_d}$ but at a slightly smaller value, as also observed for the small connectivity data in Fig. 2. We attribute this effect to the small noise that enforces v to take a small positive value. According to Eq. (9a), this reduces the asymptotic value of x by a factor of $\sqrt{1-3v^2}$. Consequently, the relative error

decreases like $1 - \sqrt{1 - 3v} \simeq 1.5\bar{v}/\lambda_d$. The trend is clearly visible in the data.

Altogether, we established an analytic description for the time evolution of the order parameter of coupled networks subject to small noise levels. For different paradigmatic network types, the collective dynamics of the network behaves just as a single aggregated tipping element with a new timescale and equilibrium values selected by the connectivity λ_d , as provided by the scaling in Eq. (8).

V. DYNAMICS AND STABILITY BEYOND THE NORMAL FORM

Up to now, we considered systems that evolve according to Eq. (2a). In this section, we explore how the dynamics changes when there are additional drift and offset terms, and how rescaling and shifting the variables x_k affects the parameters of the resulting description.

A. Influence of drift and offset terms

To discuss the impact of drift and offset terms, we write Eq. (2b) in the form of Eq. (4) with two additional terms,

$$\begin{aligned} \dot{x}_k &= \bar{x} \left(1 - \bar{x}^2 + \sum_l' d_{kl} \right) + y_k (1 - 3\bar{x}^2) - 3\bar{x}y_k^2 \\ &\quad - y_k^3 + \sum_l' d_{kl} y_l + \xi \frac{dW_k}{dt} \\ &\quad + d_k - \sum_l' d_{kl} r_{kl}. \end{aligned}$$

The terms in the first row contributed to the average of \dot{x}_k , as evaluated in Eq. (5). The terms in the second row amount to higher-order cumulants, correlations, and noise that are dropped for the closure and the weak-noise limit adopted here. The terms in the third row account for the drift and offset terms. Let the expectation of the drift terms d_k be r_D , and for the offsets r_{kl} in the coupling terms we introduce

$$\left\langle \sum_l' d_{kl} r_{kl} \right\rangle = p(N-1)d r_O = (\lambda_d - 1)r_O.$$

(Again, there may be correction terms that are subdominant for the considered closure.) With these notations, the average of \dot{x}_k takes the form

$$\dot{\bar{x}} = \bar{x}(\lambda_d - \bar{x}^2 - 3\bar{v}) + r_D - (\lambda_d - 1)r_O \quad (19)$$

and $\dot{\bar{v}}$ still takes the form of Eq. (6b). After all, the additional terms are constant such that they average to zero when multiplied by y_k . In terms of the rescaled variables [Eq. (8)], we hence find

$$\dot{x} = x(1 - x^2 - 3v) + \frac{r_D + r_O}{\lambda_d^{3/2}} - \frac{r_O}{\sqrt{\lambda_d}}, \quad (20a)$$

$$\dot{v} = 6v(\alpha - x^2). \quad (20b)$$

We note that for large connectivity $\lambda_d = 1 + pd(N-1)$, the drift and offset terms are subdominant in the order-parameter dynamics, and they disappear in the large-network

limit. Hence, the order parameter of strongly coupled large networks evolves according to Eq. (9), as discussed in Sec. III.

For large connectivity, $\lambda_d \gg 1$, every system that crosses a tipping point relaxes to its new equilibrium value according to these equations. The intrinsic order-parameter dynamics is symmetric. In terms of the effective coupling

$$r_{\text{eff}} = \frac{r_D - r_O}{\lambda_d^{3/2}} - \frac{r_O}{\sqrt{\lambda_d}}, \quad (21)$$

one encounters saddle-node bifurcations at $r_{\text{eff}} = \pm\sqrt{4/27}$ [cf. Fig. 1 and the discussion below Eq. (1)].

B. Linear coordinate transformations

Scale changes can be expressed as a change of variables where the state of the nodes is characterized by new variables z_k that are linear functions of x_k ,

$$z_k = m x_k + n \quad \text{for fixed } m, n. \quad (22)$$

Consequently, $\bar{z} = \langle z_k \rangle = m\bar{x} + n$ and $\dot{z}_k = m\dot{x}_k$. Averaging the latter equation and using Eq. (19) provides

$$\frac{\dot{\bar{z}}}{m} = \dot{\bar{x}} = \bar{x}(\lambda_d - \bar{x}^2 - 3\bar{v}) + r_D - (\lambda_d - 1)r_O.$$

For $z = \bar{z}/(m\sqrt{\lambda_d})$, $\tau = \lambda_d t$, and $z_0 = n/(m\sqrt{\lambda_d})$ we have $x = z - z_0$, and we find

$$\dot{z}(\tau) = \frac{dz}{d\tau} = (z - z_0)[1 - (z - z_0)^2 - 3v] + r_{\text{eff}}, \quad (23a)$$

$$\dot{v}(\tau) = 6v(\alpha - (z - z_0)^2) \quad (23b)$$

with a macroscopic bifurcation parameter, r_{eff} , given by Eq. (21).

The shift z_0 of z can be interpreted as a vertical displacement of the s-shaped red curve in Fig. 1. It affects the positions of the steady states, but not the bifurcation parameters. The intrinsic dynamics remains symmetric in the bifurcation parameter r_{eff} with saddle-node bifurcations at $r_{\text{crit}} = \pm\sqrt{4/27}$.

The dependence of the bifurcation parameter, Eq. (21), on connectivity λ_d provides another important insight into the stability of the networks: The drift dominates the control parameter as long as the offset terms r_{kl} are very small as compared to the drift, $(\lambda_d - 1)|r_O| \ll |r_D|$, and the global system is bistable for $-\lambda_d^{3/2} \lesssim 2.5 r_D \lesssim \lambda_d^{3/2}$ (after all $\sqrt{27/4} \approx 5/2$). In view of Eq. (7), the connectivity λ_d increases linearly with the network size such that the state of the network in this parameter range is very robust against perturbations. However, for strong connectivity the offset terms will always dominate the system response eventually,

$$(\lambda_d - 1)|r_O| \gg |r_D| \quad \text{for } \lambda_d \gg 1.$$

Eventually, the coupling terms govern the strength of the bifurcation parameter, and the range of stability increases more slowly with the connectivity

$$-\sqrt{\frac{4}{27}}\lambda_d \lesssim r_O \lesssim \sqrt{\frac{4}{27}}\lambda_d \quad \text{for } \lambda_d \gg 1.$$

Still, the range of stability increases with network size, and for increasing network size the state will become ever more robust against perturbations.

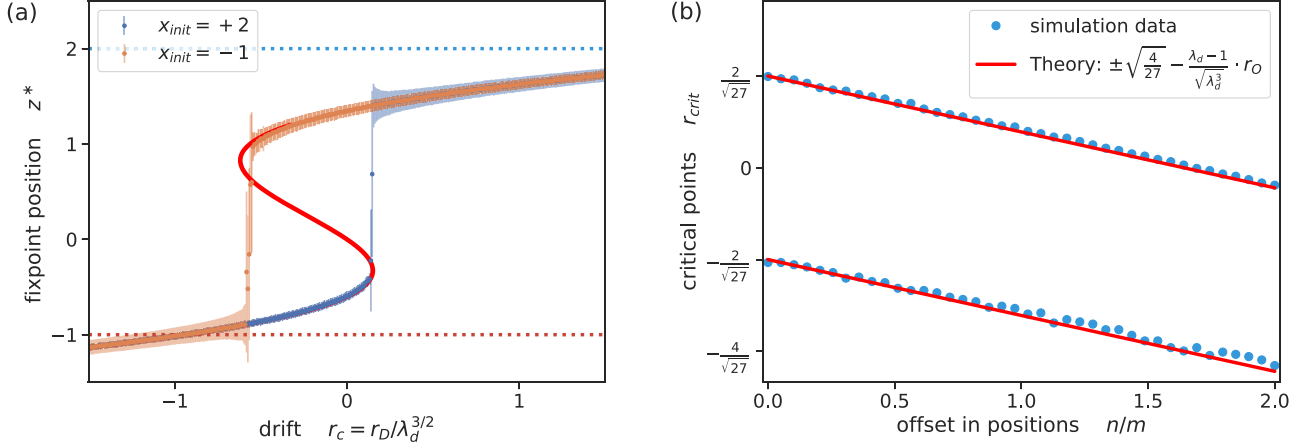


FIG. 5. Asymptotic fixed point z^* (a) and the critical points (b) for networks with an offset n and $r_{kl} = 0$ in Eq. (24). All calculations are conducted for an ER network with $N = 100$ nodes, couplings d_{kl} drawn from a uniform distribution $d_{kl} \in (0, 1.2)$, $\lambda_d = 16$, and noise strength $\xi = 0.1$. (a) For fixed values $n = m = 1$ and different drift r_D we follow the dynamics for initial conditions $x_{\text{init}} = -1$ and one excited node at $z = 1$ (orange) and $x_{\text{init}} = 2$ and one node at $z = -1$ (blue), respectively. The dots and the error bars indicate the average and the standard deviation of the late-time asymptotic positions of 50 simulations with different realizations of the network and noise. They lie nicely on the prediction for the positions of the fixed points, Eq. (25a), that is provided by the solid red line. The positions of the critical points, r_{crit} , are identified as having the largest distance between subsequent data points. (b) The n -dependence of r_{crit} determined from data as shown in panel (a), $m = 1$, and different values of n . The red lines provide the predicted positions, Eq. (25b), of the saddle-node bifurcations.

C. Coordinate transformations that do not involve the coupling

It is by no means self-evident that a change of coordinates of individual tipping elements affects the coupling terms in the same way. In particular, studies of climate networks [46] address the situation where the individual tipping elements are shifted at a *fixed* symmetric coupling. In other words, one adopts Eq. (22) but considers the dynamics

$$\begin{aligned} \frac{d}{dt} \frac{z_k}{m} = & - \left(\frac{z_k - n}{m} \right)^3 + \frac{z_k - n}{m} + d_k \\ & + \sum_l' d_{kl} (z_l - r_{kl}) + \xi \frac{dW_k}{dt} \end{aligned} \quad (24)$$

with $\langle r_{kl} \rangle = 0$. To identify the effects of this asymmetry in the parameter change, we observe that

$$\sum_l' d_{kl} (z_l - r_{kl}) = \sum_l' (m d_{kl}) \left(\frac{z_l - n}{m} - \frac{r_{kl} - n}{m} \right)$$

such that the substitution $d_{kl} \rightarrow m d_{kl}$ and $r_{kl} \rightarrow (r_{kl} - n)/m$ provides the system treated in Sec. VB. On the level of the coarse-grained system, this entails that for the present system $\lambda_d = 1 + (N - 1) p m d$ and $r_O = \langle (r_{kl} - n)/m \rangle = -n/m = -\sqrt{\lambda_d} z_0$. Substitution into Eq. (23a) provides

$$\begin{aligned} \dot{z} = & (z - z_0) [1 - (z - z_0)^2 - 3v] + \frac{r_D + r_O}{\lambda_d^{3/2}} - \frac{r_O}{\sqrt{\lambda_d}} \\ = & (z - z_0) [1 - (z - z_0)^2 - 3v] + \frac{\lambda_d - 1}{\lambda_d} z_0 + r_c \end{aligned}$$

with control parameter

$$r_c = r_D / \lambda_d^{3/2}.$$

Now, the fixed points, $\dot{z} = 0$, are located on the line

$$r_c = \frac{r_D}{\lambda_d^{3/2}} = -(z^* - z_0) [1 - (z^* - z_0)^2] - \frac{\lambda_d - 1}{\lambda_d} z_0, \quad (25a)$$

and the saddle-node bifurcations arise when

$$r_{\text{crit}} = \pm \sqrt{\frac{4}{27}} - \frac{\lambda_d - 1}{\lambda_d} z_0. \quad (25b)$$

Figure 5 demonstrates that this is indeed observed in simulations of the networks. The right-hand side of Eq. (25a) mounts to the red s-shaped curve in Fig. 5(a). The data points mark the positions of the fixed points z^* adopted by the system. For each value of z_0 we thus find a hysteresis loop that provides the critical driving parameters, r_{crit} , where the saddle-node bifurcations arise. Figure 5(b) displays the n -dependence of the positions of the saddle-node bifurcations. The data nicely follow the expected behavior, Eq. (25b), with $z_0 = n/(m\sqrt{\lambda_d})$. We conclude that incongruent response of the tipping elements and their coupling to parameter changes, as expressed by Eqs. (24) and (22), gives rise to dynamics where the system is bistable in a range of control parameters r_c that is no longer symmetric around zero.

VI. DISCUSSION AND OUTLOOK

In the main part of the present paper, we set up an analytical description of the collective tipping of a large number, N , of tipping elements that are coupled in a random network. The present section discusses these findings in the context of related literature, and it highlights prospective extensions.

A. Collective behavior

We characterized each tipping element $k \in \{1 \dots N\}$ by a scalar state variable $x_k \in \mathbb{R}$. It evolves in a double-well

potential with a saddle at $x = 0$ that separates the domains of attraction of two coexisting stable states at $x_k = \pm 1$. The elements are pairwise connected in a random network with mean coupling strength d , and a probability p that there is a connection for a given pair of elements.

The overall state of the system is characterized by the expectation \bar{x} and the variance \bar{v} of the distribution of x_k . The evolution of these collective coordinates is derived based on a closure where we drop higher-order cumulants and correlations. In the weak-noise limit, they evolve according to Eq. (6), which involves a single dimensionless parameter: the connectivity $\lambda_d = 1 + p(N - 1)d$. The coarse-grained dynamics has global fixed points at $(\bar{x}, \bar{v}) = (\pm\sqrt{\lambda_d}, 0)$, and tipping proceeds in terms of a dimensionless time $\lambda_d t$ (Fig. 2).

The dependence on $\lambda_d t$ implies that tipping occurs more abruptly for increasing network degree $p(N - 1)$ and coupling strength d . This provides a rationale for the observation of Eom [47], who also observed these trends in numerical data.

The parameter dependence of the timescale and the position of the fixed points of the collective coordinates can be absorbed by rescaling [Eq. (8)]. In line with the observations of Wunderling *et al.* [24], this implies that systems with high average degree $p(N - 1)$ only require low coupling strengths d to initiate a tipping cascade.

We have analyzed network-specific time delays in Eq. (17) and found very similar offsets for ER and WS networks of about $\Delta\tau \simeq 0.5$. Interestingly, BA networks decay with a significantly smaller time offset. We expect this to result from the existence of hubs in the BA network that could force the tipping process of the network. Follow-up work will have to clarify if and how this finding is related to the existence of hubs in the BA network.

B. Shape of the distribution

In terms of the rescaled collective coordinates $x = \bar{x}/\sqrt{\lambda_d}$ and $v = \bar{v}/\lambda_d$, the dynamics has a saddle point at position $(\alpha, (1 - \alpha^2)/3)$ with $\alpha = (3\lambda_d)^{-1/2}$. Trajectories that proceed to the right of the saddle show collective behavior. Up to initial transients, the variance of the distribution of trajectory states is small and the systems evolves according to a strongly coupled collective dynamics. Due to the assumptions taken to close the equations for x and v , the present theory does not apply for trajectories that proceed to the left of the saddle. Follow-up work will address higher-order closures in order to deal with the broad and, at times, bimodal distributions of tipping elements in this polydisperse parameter regime.

At this point, we observe that α approaches zero for increasing connectivity. Hence, a rapidly increasing fraction of initial conditions proceeds to the right of the saddle. In line with the findings of Brummitt *et al.* [16], this explains that increasing coupling strength d entails synchronous behavior of tipping elements for a larger set of initial conditions.

C. Noise

Careful inspection of our data in Fig. 4 revealed that the expectation \bar{x} saturates at values slightly below $\sqrt{\lambda_d}$. We argued that the variance \bar{v} of the distribution remains finite

for a system subjected to small noise, and that this will decrease the asymptotic value by a factor $1 - 3\bar{v}/\lambda_d$. Moreover, preliminary data indicate that noise has a nontrivial impact on the dynamics in the polydisperse parameter regime. An expansion of our model that addresses the impact of noise is in preparation.

D. Negative feedback and multiple scales

The derivation of the collective dynamics, Eqs. (6), does not involve any assumptions on the distribution of the coupling strength. The present study describes the time evolution of systems where the feedback is positive on average, $d > 0$. In this case, λ_d increases for larger and more strongly coupled networks, and the dynamics does not much depend on the structure and realization of the network (cf. Fig. 3).

For negative overall feedback, $d < 0$, and for larger networks, our connectivity as defined in Eq. (7) becomes negative and thus no longer meaningful. The nondimensionalization introduced in Eq. (8) to dimensionless parameters only works for $\lambda_d > 0$. In the case of negative overall feedback, the flow described by Eqs. (6) will always enter the realm of large \bar{v} that is out of the scope of the present assumptions for the closure of the equations. An appropriate expansion of the model will allow us to address phenomena such as Kadyrov oscillations [14,48,49].

We also expect that systems with noticeable negative feedback and vast heterogeneity in the timescales of the tipping elements and their tipping thresholds are much more susceptible to correlations of the characteristics of tipping elements and their network environment. Expansions that account for these correlations will make it possible to investigate systems like the large-scale Amazon rainforest, where spatially distant patches are dependent on each other via the atmospheric moisture recycling feedback (see, e.g., [22,24,50]). Instead of a microscale (local-scale tipping elements) and a macroscale (entire forest), one will then also define an intermediary mesoscale for strongly connected subcomponents of the forest.

E. Time dependence of parameters

The present analysis provides a comprehensive framework for the description of phase separation of networks of tipping elements for fixed-in-time control parameters. However, the Earth climate system is subjected to a sustained change of its parameters due to the release of vast amounts of carbon dioxide into the atmosphere, and on historical scales its energy input varies periodically due to Milankovitch cycles [51,52]. Both effects can have a severe impact on the time evolution. Parameter oscillations in a noisy bistable system induce stochastic resonance [53,54]. Parameter drift induces size focusing [55] as discussed recently for applications in chemistry [56] and soft biological matter [57]. Nontrivial new behavior emerges in the latter systems due to overall constraints on the dynamics due to mass conservation, or global pressure and elastic fields. It will therefore be highly relevant to explore how the dynamics is impacted by the coupling to a global parameter, like temperature in the Daisyworld models [31].

VII. CONCLUSION

In the present paper, we established a description of the collective tipping dynamics of an assembly of coupled tipping elements that are set up in a slightly perturbed unstable steady state. We described the assembly in terms of the expectation and the variance of variables that describe the state of the individual tipping elements. For a vast range of initial conditions of the network, the variance remains small throughout the evolution. In those cases, the expectation follows universal dynamics, as shown in Figs. 3 and 4 for networks with vastly different numbers of nodes, N , network degrees, $p(N - 1)$, network types (Erdős-Rényi [40], Barabási-Albert [41], and Watts-Strogatz [42]), and average coupling, d , between the elements. The dynamics is characterized by a single dimensionless parameter, λ_d , that is defined in Eq. (7). Based on the nondimensionalization, Eq. (8), it provides the timescale of the dynamics and the parameter values of the expectation and the variance of the target state of the dynamics (Fig. 2). In Sec. V we showed that the description is robust in the large network and strong coupling limit (see Fig. 5), as long as the coupling provides a positive feedback on average. Expected changes for negative feedback, $d < 0$, and other extensions of the model were briefly discussed in Sec. VI.

In conclusion, in the present work we established an effective analysis of cascading tipping behavior in strongly coupled networks. It provides a comprehensive analytical description that is in excellent agreement with numerical simulations, and it calls for extensions to address the tipping dynamics in other parameter regimes and in settings with a global feedback or other constraints.

ACKNOWLEDGMENTS

N.W. acknowledges support from the the IRTG 1740/TRP 2015/50122-0 funded by DFG and FAPESP. N.W. is grateful for support from a scholarship from the Studienstiftung des Deutschen Volkes. J.F.D. is thankful for support by the Leibniz Association (project DominoES) and the European Research Council project Earth Resilience in the Anthropocene (743080 ERA). The authors gratefully acknowledge the European Regional Development Fund (ERDF), the German Federal Ministry of Education and Research, and the Land Brandenburg for supporting this project by providing resources on the high performance computer system at the Potsdam Institute for Climate Impact Research.

-
- [1] A. Safari, R. Saidur, F. A. Sulaiman, Y. Xu, and J. Dong, A review on supercooling of phase change materials in thermal energy storage systems, *Renew. Sustainable Energy Rev.* **70**, 905 (2017).
 - [2] B. Wunderlich, One hundred years research on supercooling and superheating, *Thermochim. Acta* **461**, 4 (2007).
 - [3] K. Binder, Theory of first-order phase transitions, *Rep. Prog. Phys.* **50**, 783 (1987).
 - [4] H. Kuwahara, Y. Tomioka, A. Asamitsu, Y. Moritomo, and Y. Tokura, A first-order phase transition induced by a magnetic field, *Science* **270**, 961 (1995).
 - [5] A. Onuki, *Phase Transition Dynamics* (Cambridge University Press, Cambridge, 2002).
 - [6] R. A. da Costa, S. N. Dorogovtsev, A. V. Goltsev, and J. F. F. Mendes, Explosive Percolation Transition is Actually Continuous, *Phys. Rev. Lett.* **105**, 255701 (2010).
 - [7] R. M. D'Souza and M. Mitzenmacher, Local Cluster Aggregation Models of Explosive Percolation, *Phys. Rev. Lett.* **104**, 195702 (2010).
 - [8] R. M. D'Souza and J. Nagler, Anomalous critical and supercritical phenomena in explosive percolation, *Nat. Phys.* **11**, 531 (2015).
 - [9] P. Grassberger, C. Christensen, G. Bizhani, S.-W. Son, and M. Paczuski, Explosive Percolation is Continuous, But with Unusual Finite Size Behavior, *Phys. Rev. Lett.* **106**, 225701 (2011).
 - [10] O. Riordan and L. Warnke, Explosive percolation is continuous, *Science* **333**, 322 (2011).
 - [11] S. V. Buldyrev, R. Parshani, G. Paul, H. E. Stanley, and S. Havlin, Catastrophic cascade of failures in interdependent networks, *Nature (London)* **464**, 1025 (2010).
 - [12] A. E. Motter and M. Timme, Antagonistic phenomena in network dynamics, *Annu. Rev. Condens. Matter Phys.* **9**, 463 (2018).
 - [13] D. J. Watts, A simple model of global cascades on random networks, *Proc. Natl. Acad. Sci. (USA)* **99**, 5766 (2002).
 - [14] R. Abraham, A. Keith, M. Koebe, and G. Mayer-Kress, Computational unfolding of double-cusp models of opinion formation, *Int. J. Bifurcation Chaos* **1**, 417 (1991).
 - [15] T. M. Lenton, J. Rockström, O. Gaffney, S. Rahmstorf, K. Richardson, W. Steffen, and H. J. Schellnhuber, Climate tipping points-too risky to bet against, *Nature (London)* **575**, 592 (2019).
 - [16] C. D. Brummitt, G. Barnett, and R. M. D'Souza, Coupled catastrophes: Sudden shifts cascade and hop among interdependent systems, *J. R. Soc., Interface* **12**, 20150712 (2015).
 - [17] U. Feudel, A. N. Pisarchik, and K. Showalter, Multistability and tipping: From mathematics and physics to climate and brain—minireview and preface to the focus issue, *Chaos* **28**, 033501 (2018).
 - [18] M. Scheffer, Alternative stable states in eutrophic, shallow freshwater systems: A minimal model, *Hydrobiol. Bull.* **23**, 73 (1989).
 - [19] T. P. Hughes, S. Carpenter, J. Rockström, M. Scheffer, and B. Walker, Multiscale regime shifts and planetary boundaries, *Trends Ecol. Evol.* **28**, 389 (2013).
 - [20] T. M. Lenton and H. T. P. Williams, On the origin of planetary-scale tipping points, *Trends Ecol. Evol.* **28**, 380 (2013).
 - [21] J. C. Rocha, G. Peterson, Ö. Bodin, and S. Levin, Cascading regime shifts within and across scales, *Science* **362**, 1379 (2018).
 - [22] D. C. Zemp, C.-F. Schleussner, H. M. J. Barbosa, M. Hirota, V. Montade, G. Sampaio, A. Staal, L. Wang-Erlandsson, and A. Rammig, Self-amplified Amazon forest loss due to vegetation-atmosphere feedbacks, *Nat. Commun.* **8**, 1 (2017).
 - [23] W. Steffen, J. Rockström, K. Richardson, T. M. Lenton, C. Folke, D. Liverman, C. P. Summerhayes, A. D. Barnosky, S. E.

- Cornell, M. Crucifix *et al.*, Trajectories of the Earth system in the Anthropocene, *Proc. Natl. Acad. Sci. (USA)* **115**, 8252 (2018).
- [24] N. Wunderling, B. Stumpf, J. Krönke, A. Staal, O. A. Tuinenburg, R. Winkelmann, and J. F. Donges, How motifs condition critical thresholds for tipping cascades in complex networks: Linking micro-to macro-scales, *Chaos* **30**, 043129 (2020).
- [25] J. Krönke, N. Wunderling, R. Winkelmann, A. Staal, B. Stumpf, O. A. Tuinenburg, and J. F. Donges, Dynamics of tipping cascades on complex networks, *Phys. Rev. E* **101**, 042311 (2020).
- [26] J. Garbe, T. Albrecht, A. Levermann, J. F. Donges, and R. Winkelmann, The hysteresis of the Antarctic ice sheet, *Nature (London)* **585**, 538 (2020).
- [27] A. Robinson, R. Calov, and A. Ganopolski, Multistability and critical thresholds of the greenland ice sheet, *Nat. Clim. Change* **2**, 429 (2012).
- [28] J. A. Curry, J. L. Schramm, and E. E. Ebert, Sea ice-albedo climate feedback mechanism, *J. Clim.* **8**, 240 (1995).
- [29] M. Müller-Stoffels and R. Wackerbauer, Regular network model for the sea ice-albedo feedback in the arctic, *Chaos* **21**, 013111 (2011).
- [30] E. Kriegler, J. W. Hall, H. Held, R. Dawson, and H. J. Schellnhuber, Imprecise probability assessment of tipping points in the climate system, *Proc. Natl. Acad. Sci. (USA)* **106**, 5041 (2009).
- [31] A. J. Watson and J. E. Lovelock, Biological homeostasis of the global environment: The parable of Daisyworld, *Tellus B* **35**, 284 (1983).
- [32] M. I. Budyko, The effect of solar radiation variations on the climate of the Earth, *Tellus* **21**, 611 (1969).
- [33] W. D. Sellers, A global climatic model based on the energy balance of the Earth-atmosphere system, *J. Appl. Meteorol. Climatol.* **8**, 392 (1969).
- [34] P. F. Hoffman, A. J. Kaufman, G. P. Halverson, and D. P. Schrag, A neoproterozoic snowball Earth, *Science* **281**, 1342 (1998).
- [35] V. Lucarini and T. Bódai, Transitions Across Melancholia States in a Climate Model: Reconciling the Deterministic and Stochastic Points of View, *Phys. Rev. Lett.* **122**, 158701 (2019).
- [36] H. B. Callen, *Thermodynamics and an Introduction to Thermostatistics* (Wiley, New York, 1985).
- [37] N. Wunderling, J. Krönke, V. Wohlfarth, J. Kohler, J. Heitzig, A. Staal, S. Willner, R. Winkelmann, and J. F. Donges, Modelling nonlinear dynamics of interacting tipping elements on complex networks: The pycascades package, *Eur. Phys. J.: Spec. Top.* (2021).
- [38] A. K. Klose, V. Karle, R. Winkelmann, and J. F. Donges, Emergence of cascading dynamics in interacting tipping elements of ecology and climate, *R. Soc. Open Sci.* **7**, 200599 (2020).
- [39] J. Murdock, Normal forms, *Scholarpedia* **1**, 1902 (2006).
- [40] P. Erdős and A. Rényi, On random graphs, *Publ. Math.* **6**, 290 (1959).
- [41] A.-L. Barabási and R. Albert, Emergence of scaling in random networks, *Science* **286**, 509 (1999).
- [42] D. J. Watts and S. H. Strogatz, Collective dynamics of 'small-world' networks, *Nature (London)* **393**, 440 (1998).
- [43] A. Hagberg, P. Swart, and D. S. Chult, Exploring network structure, dynamics, and function using NetworkX, Tech. Rep. (Los Alamos National Lab., Los Alamos, NM, 2008).
- [44] M. J. Aburn, sdeint: Numerical integration of stochastic differential equations (SDE), software available under GNU general public license (2017), accessed: 2020-07-18.
- [45] V. I. Arnold, *Catastrophe Theory*, 3rd ed. (Springer, Berlin, 1992).
- [46] N. Wunderling, J. F. Donges, J. Kurths, and R. Winkelmann, Interacting tipping elements increase risk of climate domino effects under global warming, *Earth Syst. Dyn.* **12**, 601 (2021).
- [47] Y.-H. Eom, Resilience of networks to environmental stress: From regular to random networks, *Phys. Rev. E* **97**, 042313 (2018).
- [48] M. N. Kadyrov, A mathematical model of the relations between two states, in *Global Development Processes: Modeling and Analysis*, Collected Papers Vol. 3 (Institute for System Studies, Moscow, 1984), pp. 87–99.
- [49] N. Wunderling, M. Gelbrecht, R. Winkelmann, J. Kurths, and J. F. Donges, Basin stability and limit cycles in a conceptual model for climate tipping cascades, *New J. Phys.* **22**, 123031 (2020).
- [50] A. Staal, O. A. Tuinenburg, J. H. C. Bosmans, M. Holmgren, E. H. van Nes, M. Scheffer, D. C. Zemp, and S. C. Dekker, Forest-rainfall cascades buffer against drought across the Amazon, *Nat. Clim. Change* **8**, 539 (2018).
- [51] J. D. Hays, J. Imbrie, and N. J. Shackleton, Variations in the earth's orbit: Pacemaker of the ice ages, *Science* **194**, 1121 (1976).
- [52] A. L. Sørensen, A. T. Nielsen, N. Thibault, Z. Zhao, N. H. Schovsbo, and T. W. Dahl, Astronomically forced climate change in the late cambrian, *Earth Planet. Sci. Lett.* **548**, 116475 (2020).
- [53] R. Benzi, G. Parisi, A. Sutera, and A. Vulpiani, Stochastic resonance in climatic change, *Tellus* **34**, 10 (1982).
- [54] L. Gammaitoni, P. Hänggi, P. Jung, and F. Marchesoni, Stochastic resonance, *Rev. Mod. Phys.* **70**, 223 (1998).
- [55] J. Vollmer, A. Papke, and M. Rohloff, Ripening and focusing of aggregate size distributions with overall volume growth, *Front. Phys.* **2**, 18 (2014).
- [56] M. D. Clark, S. K. Kumar, J. S. Owen, and E. M. Chan, Focusing nanocrystal size distributions via production control, *Nano Lett.* **11**, 1976 (2011).
- [57] K. A. Rosowski, T. Sai, E. Vidal-Henriquez, D. Zwicker, R. W. Style, and E. R. Dufresne, Elastic ripening and inhibition of liquid-liquid phase separation, *Nat. Phys.* **16**, 422 (2020).